THE JOURNAL OF PHYSICAL CHEMISTRY B

ARTICLE

pubs.acs.org/JPCB

Mechanism of Recombination of the $P^+H_A^-$ Radical Pair in Mutant *Rhodobacter sphaeroides* Reaction Centers with Modified Free Energy Gaps Between $P^+B_A^-$ and $P^+H_A^-$

Krzysztof Gibasiewicz,[*,†] Maria Pajzderska,[†] Jane A. Potter,[‡,⊥] Paul. K. Fyfe,[‡,#] Andrzej Dobek,[†] Klaus Brettel,[§,∥] and Michael R. Jones[‡]

[†]Department of Physics, Adam Mickiewicz University, ul. Umultowska 85, 61-614 Poznań, Poland

[‡]School of Biochemistry, Medical Sciences Building, University of Bristol, University Walk, Bristol, BS8 1TD, United Kingdom

[§]CEA Saclay, IBITECS, Laboratoire de Photocatalyse et Biohydrogène, 91191 Gif-sur-Yvette, France

[∥]CNRS, URA2096, 91191 Gif-sur-Yvette, France

ABSTRACT: The kinetics of recombination of the $P^+H_A^-$ radical pair were compared in wild-type reaction centers from *Rhodobacter sphaeroides* and in seven mutants in which the free energy gap, ΔG, between the charge separated states $P^+B_A^-$ and $P^+H_A^-$ was either increased or decreased. Five of the mutant RCs had been described previously, and X-ray crystal structures of two newly constructed complexes were determined by X-ray crystallography. The charge recombination reaction was accelerated in all mutants with a smaller ΔG than in the wild-type, and was slowed in a mutant having a larger ΔG. The free energy difference between the state $P^+H_A^-$ and the PH_A ground state was unaffected by most of these mutations. These observations were consistent with a model in which the $P^+H_A^- \rightarrow PH_A$ charge recombination is thermally activated and occurs via the intermediate state $P^+B_A^-$, with a mean rate related to the size of the ΔG between the states $P^+B_A^-$ and $P^+H_A^-$ and not the ΔG between $P^+H_A^-$ and the ground state. A more detailed analysis of charge recombination in the mutants showed that the kinetics of the reaction were multiexponential, and characterized by ~0.5, ~1−3, and 7−17 ns lifetimes, similar to those measured for wild-type reaction centers. The exact lifetimes and relative amplitudes of the three components were strongly modulated by the mutations. Two models were considered in order to explain the observed multiexponentiality and modulation, involving heterogeneity or relaxation of $P^+H_A^-$ states, with the latter model giving a better fit to the experimental results.

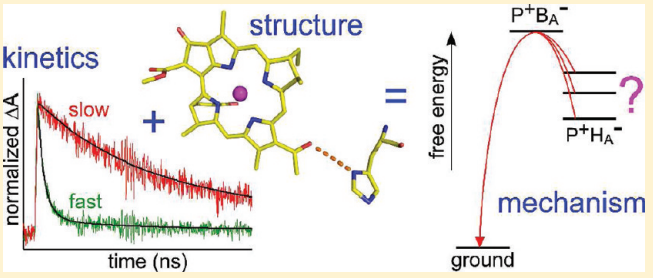

INTRODUCTION

Charge separation in reaction centers (RCs) from purple photosynthetic bacteria such as *Rhodobacter* (*Rba.*) *sphaeroides* comprises an initial electron transfer from the primary electron donor, a bacteriochlorophyll (BChl) dimer (P), to the primary electron acceptor, a bacteriopheophytin (BPhe - H_A), forming the radical pair $P^+H_A^-$ (Figure 1). This is followed by further electron transfer from the reduced H_A^- to a ubiquinone (Q_A). In native RCs, the primary charge separation occurs in ~3−6 ps and the subsequent charge stabilization in ~200−300 ps (see reviews[1,2]). As depicted in Figure 1A, a monomeric BChl (B_A) is located between the P dimer and H_A, and this was proposed to mediate electron transfer between the two either as a real anion intermediate[3,4] or by acting as a virtual electron transfer carrier.[5−9] When forward electron transfer from H_A^- to Q_A is blocked, charge recombination from H_A^- to P^+ is observed[10−16] (see also reviews[1,17]). Charge recombination proceeds to a very minor extent via repopulation of the excited state of the P dimer (P*), detectable by its delayed fluorescence, but in the main fraction of RCs recombination leads directly to the ground singlet states of P and H_A without formation of an excited state. With a certain probability, an intermediate formation of the triplet excited state of the P dimer (^{3}P) also occurs.[10,17,18] Forward electron transfer from H_A^- to Q_A may be blocked either by prereducing Q_A to Q_A^- (chemically using a strong reductant such as sodium dithionite[10,11] or by illumination in the presence of a weaker reductant[15,16]) or by its biochemical removal[10−14] or genetic removal.[19,20] RCs with such a block in electron transfer are described as "closed".

Recombination of the $P^+H_A^-$ charge separated state has been studied in a number of species of purple bacteria by transient absorption[10−14] and time-resolved fluorescence.[18,21] Until recently, there was a consensus that this reaction could be well described by a single exponential lifetime of ~15 ns when studied by transient absorption, whereas in fluorescence three phases have been resolved with lifetimes of <1, ~3, and ~12 ns.[18,21] The exact values of these lifetimes and their relative amplitudes could be modulated to a moderate extent by an external magnetic field,

Received: July 8, 2011
Revised: October 3, 2011
Published: October 04, 2011

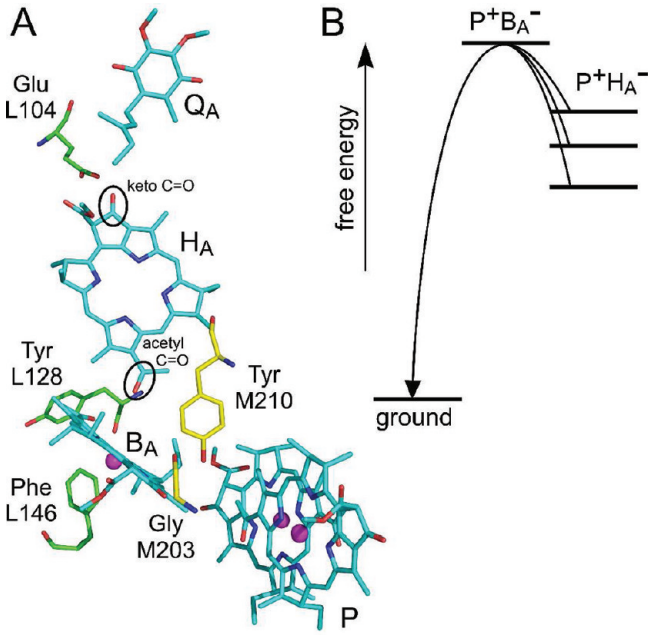

Figure 1. Structure of the *Rba. sphaeroides* RC and the energetics of charge recombination. (A) Structure of the electron transfer cofactors in the active branch of the *Rba. sphaeroides* RC (P dimer, B_A, H_A, and Q_A – cyan carbons) and the five residues targeted by site-directed mutagenesis in the L-polypeptide (green carbons) or M-polypeptide (yellow carbons). For other atoms, red = oxygen, blue = nitrogen, and magenta sphere = magnesium. (B) A simplified model scheme of the free energy of the charge separated states $P^+B_A^-$ and $P^+H_A^-$ in the *Rba. sphaeroides* RC. A ladder of three different free energy levels of the state $P^+H_A^-$ gives rise to the observed three-exponential kinetics of $P^+H_A^- \rightarrow PH_A$ charge recombination. The three $P^+H_A^-$ levels may represent different subpopulations of RCs (heterogeneity model) or may be viewed as consecutive temporal states in a homogeneous population of RCs (relaxation model).

the state of Q_A, the concentration of RCs, the composition of the buffer, and temperature.[17,18,21] The apparent discrepancy in the kinetic complexity observed between absorption and fluorescence data was explained by a model in which the $P^+H_A^-$ state stabilizes in time (relaxes) relative to P*, giving rise to a multiexponential decay in fluorescence measurements but not in transient absorption.[21]

Recently, multiexponential kinetics of $P^+H_A^-$ recombination in purified *Rba. sphaeroides* RCs were also observed by transient absorption,[15,16] and it was reported that the kinetics were modulated by the state of the Q_A quinone. When Q_A was removed, the recombination was much slower (lifetime of the order of 12 ns) than if it was prereduced to Q_A^-. In the latter case, the charge recombination was clearly multiexponential, with three resolved phases similar to those reported in time-resolved fluorescence studies: lifetimes were <1, ~3−4, and ~12 ns, the last of these matching the lifetime observed in RCs without Q_A. The mean lifetime for Q_A-reduced RCs was ~5 ns. Addition of *o*-phenanthroline, a herbicide that docks in the Q_B site and is known to modify the p*K* values of amino acids,[22] had a minor effect on the charge recombination rate in Q_A-removed RCs but significantly slowed this reaction in Q_A-reduced RCs (mean lifetime was increased to ~9 ns). All of these results were interpreted within the framework of a model which envisages a ladder of free energy levels for the state $P^+H_A^-$ (Figure 1B).[15,16] In Q_A-removed RCs, mainly the lowest level is populated, whereas up to three levels are more evenly populated in Q_A-reduced RCs, both with and without *o*-phenanthroline (Figure 1B). The increased population of higher-energy levels of $P^+H_A^-$ in Q_A-reduced RCs was explained by the presence of an electrostatic interaction between the negative charges on Q_A^- and H_A^-. The underlying basis of multiple energy levels for the state $P^+H_A^-$ was tentatively assigned to a structural heterogeneity within the RC population originating from different protonation states of a few amino acid residues that modulate this electrostatic interaction.[15,16]

An alternative relaxation model[21] has also been adopted recently to explain multiphasic charge recombination.[16] In this model, the free energy gap between $P^+B_A^-$ and $P^+H_A^-$ is proposed to increase with time, a change which also leads to a distribution of charge recombination lifetimes. The rate of this increase affects the overall kinetics of the charge recombination. It was concluded that, independent of the model, the higher the free energy of $P^+H_A^-$ above the ground state, the faster the charge recombination. Since electrostatic repulsion of the charge on Q_A^- would be expected to push the free energy of $P^+H_A^-$ up toward that of $P^+B_A^-$ and since the B_A BChl is situated between the P BChl dimer and the H_A BPhe in the RC, it was natural to propose that recombination of $P^+H_A^-$ occurs via a thermally activated $P^+B_A^-$ state. However, it can also be argued that the charge recombination to the ground state occurs directly from the state $P^+H_A^-$ and that the observed modulation of the kinetics of this reaction results from a distribution of free energy gaps between the state $P^+H_A^-$ and the ground state, in line with the driving force dependence of the electron transfer rate as predicted in classical electron transfer theory.[23]

To further explore the role of B_A in the recombination of $P^+H_A^-$ and to test the hypothesis that this reaction occurs via a thermally activated repopulation of the $P^+B_A^-$ state, in the present work, transient absorption measurements were conducted on a series of mutant *Rba. sphaeroides* RCs with a modified free energy gap between $P^+B_A^-$ and $P^+H_A^-$ and, in most cases, an unchanged free energy gap between $P^+H_A^-$ and the PH_A ground state. Seven single-residue mutations were employed that are known, or proposed, to alter the characteristics of primary electron transfer and charge recombination through effects on the reduction potentials of B_A and H_A. In five cases, these effects are mediated through the introduction or removal of hydrogen bonds between the protein and the acetyl or keto carbonyl substituents of B_A or H_A; these substituents are circled for H_A in Figure 1A. Two of these mutations have not been described previously, and their X-ray crystal structures were determined. Findings are discussed in the context of models that envisage either a static distribution of free energies for $P^+H_A^-$ or a time-dependent decrease in this free energy.

EXPERIMENTAL METHODS

Construction of Mutant Strains. Tyr 128 of the L-polypeptide of the *Rba. sphaeroides* RC was mutated to His (denoted YL128H), and Phe 146 of this polypeptide was mutated to Ala (FL146A). The YL128H and FL146A mutations were constructed using the QuikChange method (Stratagene), using plasmid pUCXB-1 as the template.[24] Mutations were restricted to the target codon and confirmed by DNA sequencing. Restriction fragments containing the mutations were shuttled into expression vector pRKEH10D[25] and expressed in *Rba. sphaeroides*

Table 1. Crystallographic Statistics for Data Collection and Refinement

reaction center (PDB entry)	FL146A (3ZUM)	YL128H (3ZUW)
	Collection Statistics	
resolution range	12.0−2.5	17.9−2.3
no. of unique reflections	68081	85753
completeness (%)	99.1	98.0
R_{merge}[a] (%)	7.5	7.3
	Refinement Statistics	
R factor[b] (%)	19.5	19.2
R_{free}[c] (%)	22.8	22.4
	Geometry	
coord error[d] (Å)	0.22	0.17
rmsd from ideality		
bonds	0.018	0.021
angles	2.03	2.14
Ramachandran plot[e]		
most favored	96.1	96.8
additional allowed	3.7	2.9
disallowed	0.2	0.2
no protein residues	817	823
cofactors	4 BChl, 2 BPhe, 2 Ubi, 1 Fe, 1 Spn	4 BChl, 2 BPhe, 2 Ubi, 1 Fe, 1 Spn
waters	206	298
detergents (LDAO)	7	9
lipids	0	0
others	2 phosphates	2 phosphates

[a] $R_{merge} = \Sigma_h\Sigma_i|\langle I(h)\rangle - I(h)_i|/\Sigma_h\Sigma_i I(h)_i$, where $I(h)$ is the intensity of the reflection h, Σ_h is the sum over all reflections, and Σ_i is the sum over all i measurements of reflection h. [b] The R factor is defined by $\Sigma||F_o| - |F_c||/|F_o|$. [c] R_{free} was calculated with 5% reflections selected randomly.[62] [d] Coordinate error was estimated with Cruickshank's DPI.[63] [e] The Ramachandran plot was generated using the program Procheck version 3.[64]

deletion strain DD13.[26] This produced transconjugant strains that had mutant RCs but lacked both types of *Rba. sphaeroides* light-harvesting complexes.[26]

Preparation of RCs for Analysis. Antenna-deficient strains of *Rba. sphaeroides* assembling wild-type (WT) or mutant RCs were grown under dark/semiaerobic conditions as described elsewhere,[26] and intracytoplasmic membranes were isolated by breakage of harvested cells in a French pressure cell, followed by purification on 15%/40% (w/v) sucrose density step gradients.[27]

RCs were purified for structure determination as described in detail previously.[24] Briefly, the procedure employed solubilization of the RC in lauryldimethylamine oxide (LDAO) followed by three anion exchange chromatographic steps, two using DE52 media (Whatman), one using Sepharose Q media (Pharmacia), and a final gel filtration step using a Sephadex 200 preparative grade column (Pharmacia).

X-ray Crystallography. Trigonal crystals of the *Rba. sphaeroides* RC with space group $P3_121$ were grown by sitting drop vapor diffusion from droplets containing 9 mg/mL RC, 0.09% v/v LDAO, 3.5% w/v 1,2,3-heptanetriol, and 0.75 M potassium phosphate (pH 7.5).[24] The drops were equilibrated against a reservoir of 1.5 M potassium phosphate. Trigonal crystals appeared within 4 weeks and grew as prisms of variable size, ranging from 0.5 to 2.0 mm in the longest dimension. The crystals had approximate unit cell dimensions of $a = b = 138$ Å, $c = 184$ Å, $\alpha = \beta = 90°$, and $\gamma = 120°$.

X-ray diffraction data were collected at 100 K on a ADSC Quantum 4R CCD detector on station 14.1 of the Daresbury Synchrotron Radiation Source. Crystals were removed from the well and washed in artificial mother liquor. The crystals were then moved sequentially through liquors with increasing concentrations of glycerol to reach a final glycerol concentration of 35%. Diffraction data were processed using the HKL2000 package.[28] Collection and refinement statistics are given in Table 1. Molecular replacement was performed using AMORE[29] using the coordinates of the WT RC[24] as a starting model. This was followed by refinement using REFMAC 5.[30] In the figures, structures were illustrated using PyMOL.[31]

Transient Absorption Measurements. For the transient absorption experiments, concentrated antenna-deficient membranes containing WT or mutant RCs were diluted in 15 mM Tris buffer (pH 8), containing 0.025% LDAO, and placed in a quartz cell with 10 mm optical path for the monitoring light and 2 mm for the excitation beam. The typical final optical density of the samples was $OD_{800nm,1cm} = 0.7$. In order to keep the Q_A-containing RCs in the state with Q_A permanently reduced (Q_A^-), the samples were illuminated during the transient absorption measurements by continuous background white light (~1 mW/cm^2) in the presence of an efficient electron donor (7.5 mM sodium ascorbate) and 7.5 mM *o*-phenanthroline which prevented electron transfer from Q_A^- to Q_B. In the case of the Q_A-deficient mutant AM260W, only sodium ascorbate was added and background light was not applied.

Transient absorption measurements were performed using the setup described in Byrdin et al.[32] Briefly, vertically polarized saturating excitation flashes of ~2 mJ energy and of 100 ps

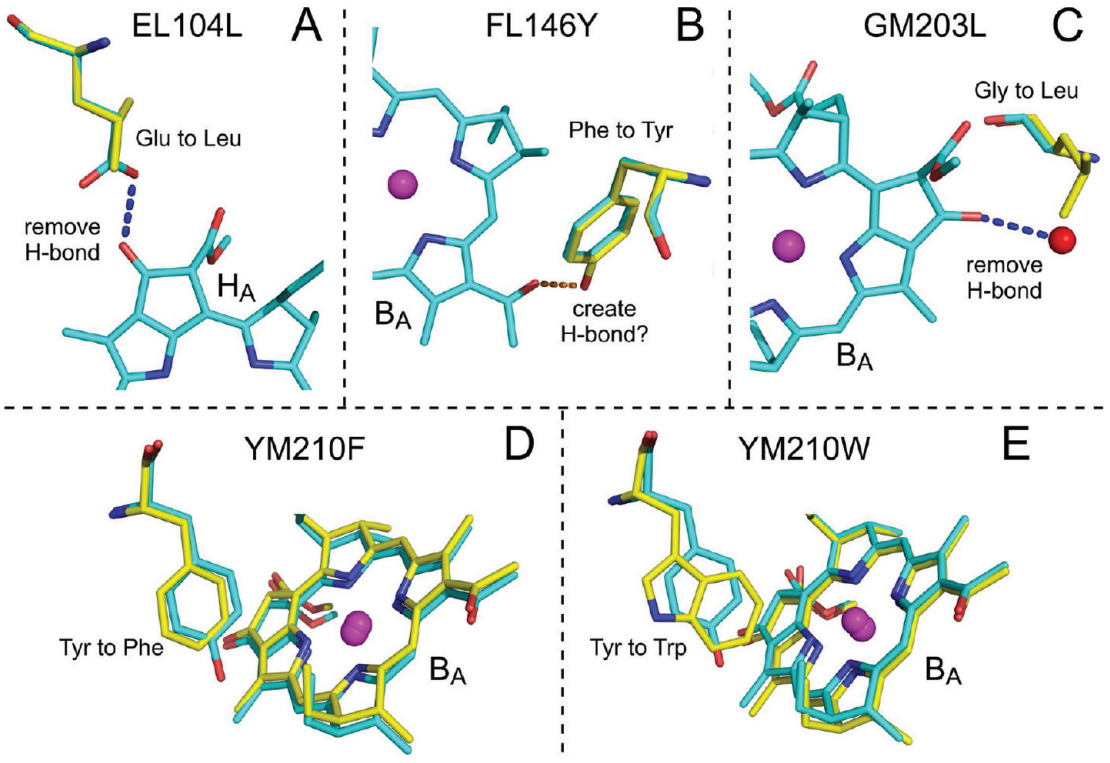

Figure 2. Key structural consequences of previously reported RC mutations. Overlaid structures of WT and mutant RCs are shown with cyan and yellow carbons, respectively. (A) *In silico* model showing how the hydrogen bond (blue dots) donated by Glu L104 to the keto carbonyl of the H_A BPhe is lost on mutation to Leu. (B) *In silico* model showing how a hydrogen bond (orange dots) could be donated to the acetyl carbonyl of B_A by mutation of Phe L146 to Tyr. (C) Overlay of X-ray crystal structures of the WT RC and GM203L RC (PDB entry 2BOZ[41]); the Leu side chain in the GM203L mutant sterically excludes the native water (red sphere) that donates a hydrogen bond (blue dots) to the keto carbonyl of B_A. (D) Overlay of X-ray crystal structures of the WT RC and the YM210F RC (PDB entry 1YF6[51]), showing loss of the phenolic OH group on replacement of Tyr M210 by Phe. (E) Overlay of X-ray crystal structures of WT RC and the YM210W RC[53] showing a small shift in the position of B_A to accommodate the bulkier Trp. The simple *in silico* models of the mutant RCs in parts A and B were generated using the structure of the WT RC and the mutate function of PyMOL.[31]

duration at 532 nm were provided by a Nd:YAG laser (Continuum Leopard SS-10) at a repetition rate of ~2 Hz. An external cavity diode laser system (EOSI 2010) was used as the analyzing light source at 690 nm. In order to minimize the excitation effect of the monitoring light, it was chopped with a frequency of 206 Hz, such that the monitoring light passed through the sample every ~5 ms for 140 μs. The detection system consisted of a fast photodiode (rise time 200 ps; model UPD-200-UP from Alphalas) and a digitizing oscilloscope (Agilent Infinium 81004B; 10 GHz; sampling rate, 40 Gsamples/s), which allowed a time resolution of about 300 ps. All experiments were made at room temperature in a 6 μs temporal window.

Transient absorption kinetic traces were fitted with the sum of up to three exponential functions plus a constant using the program Origin. The fitting was performed separately in the 100 ns and 6 μs windows. The starting point of the fits was always at the maximum of the experimental kinetic traces.

RESULTS

Effects of Mutation on the Properties of H_A and B_A. The subnanosecond spectroscopy described below employed seven RCs with single point mutations in the vicinity of H_A or B_A; the locations of the residues concerned are shown in Figure 1A. Five of these have been described previously and their effects characterized through a combination of spectroscopy and, in three cases, X-ray crystallography. The key structural changes associated with these five mutations are summarized in Figure 2. An eighth RC with a single point mutation that causes the complex to assemble without a Q_A quinone (Ala M260 to Trp – AM260W) was also studied, and the structural and spectroscopic properties of this complex have been reported in detail.[19,20,33]

In the EL104L RC, it is generally accepted that substitution of Glu L104 with Leu removes a hydrogen bond interaction with the H_A BPhe.[34] An *in silico* model of this mutation is shown in Figure 2A; in the WT RC, a protonated Glu side chain (cyan carbons) donates a hydrogen bond (blue dots) to the keto carbonyl of H_A, but this is lost on mutation to Leu (yellow carbons). Loss of this hydrogen bond would be expected to selectively raise the free energy of $P^+H_A^-$ by lowering the redox potential of H_A/H_A^-, as depicted graphically in Figure 3. This expectation is based on the generally observed trend that the addition of a hydrogen bond to the acetyl or keto carbonyl groups of the P BChls increases the midpoint redox potential (E_m) of the P/P^+ couple, and thus stabilizes the charge separated states involving P^+, whereas removing a hydrogen bond to P has the opposite effect.[35] For EL104L and the mutants described below, a similar logic was applied when predicting the effects of addition or removal of hydrogen bonds to B_A or H_A. In support of expectations regarding the EL104L mutant, data from low temperature absorbance spectroscopy, linear dichroism, resonance Raman, FTIR difference spectroscopy, and ENDOR

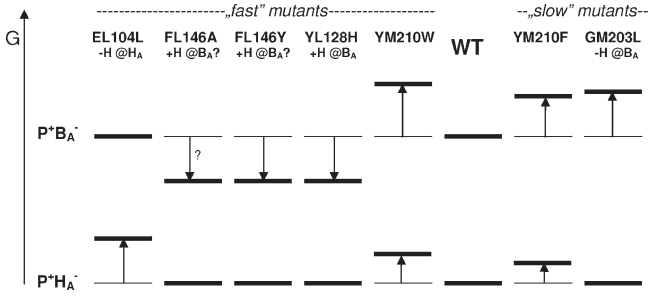

Figure 3. Overview of the expected free energy shifts of the states $P^+H_A^-$ and $P^+B_A^-$ resulting from the single point mutations near H_A and B_A. The RCs are ordered from those with fastest charge recombination kinetics on the left to those with slowest on the right. Mutations which remove a hydrogen bond either from H_A or B_A (labeled −H @H_A and −H @B_A, respectively) are expected to increase the free energy of the respective state $P^+H_A^-$ or $P^+B_A^-$ (EL104L and GM203L, respectively). Mutations which add a hydrogen bond to B_A (labeled +H @B_A) are expected to lower the free energy of $P^+B_A^-$ (YL128H and likely FL146Y and FL146A). Mutations of Tyr M210 are not expected to add or remove any hydrogen bonds. However, they are known to increase the redox potential of P/P^+ [42−44,48−50] and they were proposed to destabilize B_A^-.[40,46,47] As a consequence, the free energy of both $P^+H_A^-$ and $P^+B_A^-$ is expected to be shifted up with a net effect of increase in the free energy gap between these two states. See text for further details.

spectroscopy have revealed an influence of this Glu on the properties of the H_A keto carbonyl (see the Discussion and references in ref 36), and replacement of this Glu by Leu is known to modulate this influence.[34,37,38] This mutation brings about modest slowing of the rates of P* decay (time constant of 3.4 ps in the WT changes to 4.8 ps in the mutant) and $H_A^- \rightarrow Q_A$ electron transfer (238 to 270 ps).[34]

Structural modeling suggests that substitution of Phe L146 with Tyr in the FL146Y RC could lead to formation of a hydrogen bond between the Tyr hydroxyl and the acetyl carbonyl of B_A (Figure 2B), selectively lowering the free energy of $P^+B_A^-$, as depicted in Figure 3. Conversely, it has been suggested that $P^+B_A^-$ could be stabilized by the introduction of an OH dipole[39] in a manner similar to that proposed for the interaction between Tyr M210 and B_A.[40] Schenkl et al.[39] have reported that the FL146Y mutation brings about small acceleration of $P^* \rightarrow P^+B_A^-$ (3.5 to 2.9 ps) but does not change the rate of the $H_A^- \rightarrow Q_A$ step. It has a selective effect on the $B_A^- \rightarrow H_A$ transfer, which becomes biphasic (from a time constant of 1 ps (100%) in the WT RC to 1 ps (70%) and 8 ps (30%) in the mutant).

Mutation of Gly M203 to Leu (GM203L) brings about an ∼8-fold slowing in the rate of P* decay,[41] and this is accompanied by the removal of a hydrogen bond interaction between the keto carbonyl of B_A and an adjacent water molecule (Figure 2C). An X-ray crystal structure at a resolution of 2.4 Å showed that the bulkier Leu side chain excludes this water from the structure of the GM203L RC,[41] breaking this stabilizing hydrogen bond and providing a mechanism for an increase in the free energy of $P^+B_A^-$ (Figure 3).

Finally, mutations of the Tyr side chain at the M210 position to Phe and Trp are known to increase E_m P/P^+ by a few tens of mV,[42−45] which will increase the free energy of both $P^+B_A^-$ and $P^+H_A^-$ by equivalent amounts. However, these mutations have very strong slowing effects on the rate of primary charge separation, the size of which cannot be simply attributed to changes in the redox potential of P/P^+. This has been explained through proposals that the OH dipole of the native Tyr has a strong stabilizing effect on the adjacent B_A anion, and that replacement by Phe in aYM210F RC will further raise the free energy of $P^+B_A^-$.[40,46,47] In the YM210F mutant (Figure 2D), an approximate 5-fold slowing in the rate of P* decay has been observed with an ∼30 mV increase in E_m P/P^+,[42−44,48−50] and an X-ray crystal structure at a resolution of 2.25 Å of a RC with the YM210F mutation[51] has shown that the structural change is restricted to loss of the Tyr OH group, the orientation of the Phe ring being similar to that of the native Tyr (Figure 2D). In the case of the YM210W RC, the rate of P* decay is slowed by 12- to 15-fold,[43,44,52] again due to an ∼50 mV increase in E_m for P/P^+ and loss of the native Tyr (Figure 2E). In addition, X-ray crystallography has shown an additional small shift in the degree of tilt of the B_A macrocycle, caused by replacement of Tyr by a bulkier Trp, that may contribute to even slower charge separation in this RC compared to the YM210F complex.[53] In these two RCs, an increase in the free energy difference between $P^+B_A^-$ and $P^+H_A^-$ is therefore expected as a result of destabilization of B_A^-, on top of a rise in the absolute free energy of both radical pairs due to destabilization of P^+ (Figure 3).

X-ray Crystal Structures of New Mutant RCs. In addition to these previously characterized RCs, in the present work, two new mutants were constructed and their X-ray crystal structures determined. Both mutations, Tyr L128 to His (YL128H) and Phe L146 to Ala (FL146A), were made with the intention of selectively stabilizing the $P^+B_A^-$ radical pair through an effect on B_A. The X-ray crystal structures of these two mutant RCs were determined as described in the Experimental Methods section, to resolutions of 2.3 and 2.5 Å, respectively. Statistics for data collection and structure refinement are given in Table 1.

The YL128H mutation was introduced with a view to introducing a hydrogen bond to the acetyl carbonyl of B_A. Comparison of the X-ray crystal structure of the YL128H mutant with that of the WT RC showed that the imidazole ring of the introduced His was arranged approximately coplanar with the phenol ring of the replaced Tyr (Figure 4A), with no significant disturbance to the structure of the surrounding protein−cofactor system, including the orientation of the adjacent acetyl carbonyl group of B_A relative to the plane of the macrocycle. Figure 4B shows a stereo view of the electron density map and fitted structure for B_A and His L128; as can be seen, the ND nitrogen of His L128 was in a suitable position to donate a hydrogen bond to the oxygen of the acetyl carbonyl of B_A, at a N-to-O distance of 3.6 Å (orange dots in Figure 4B). This arrangement was consistent with the aim of lowering the free energy of $P^+B_A^-$, as shown schematically in Figure 3.

As outlined above, Shenkl and co-workers[39] have mutated residue Phe L146 to Tyr with a view to also introducing a hydrogen bond to the acetyl carbonyl of B_A, and a model of how this might be achieved is shown in Figure 2B. In addition to reproducing this FL146Y mutation, in the present work, this Phe was also mutated to Ala (FL146A) with the aim of creating an intraprotein cavity that could house one or more water molecules that could act as a hydrogen bond donor to the acetyl carbonyl of B_A. Such an interaction would mirror the water-mediated hydrogen bond at the keto carbonyl of B_A that is removed in the GM203L RC.[41] Comparison of the X-ray crystal structure of the FL146A mutant with that of the WT RC showed that a cavity was indeed created, with no significant disturbance to the surrounding protein. Figure 4C shows a stereo view of the

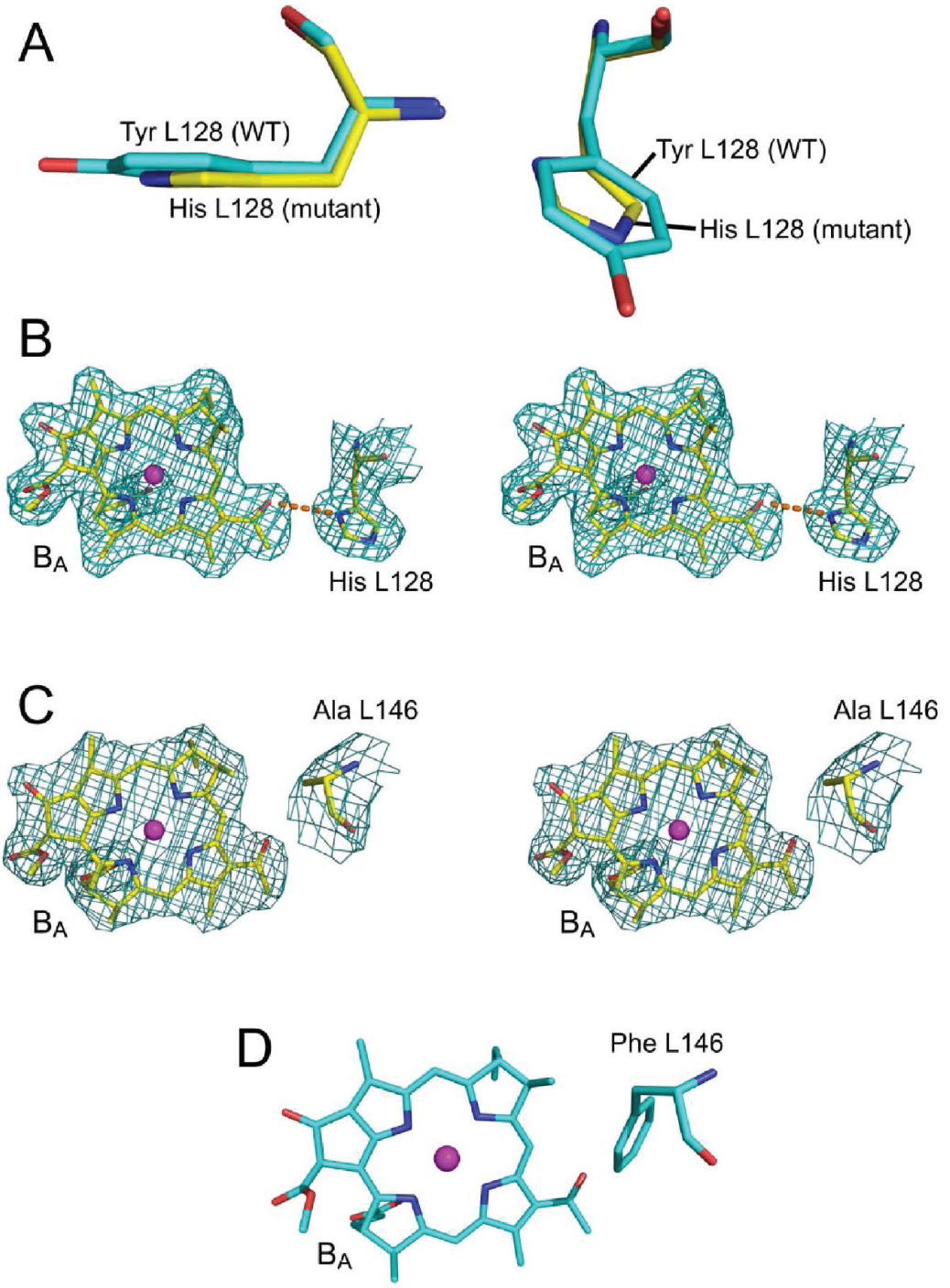

Figure 4. Structural analysis of the YL128H and FL146A RCs. (A) Backbone alignment of the X-ray structures of the WT (cyan carbons) and YL128H (yellow carbons) RCs, showing the approximately coplanar arrangement of the L128 residue in the two structures (red = oxygen, blue = nitrogen). (B) Stereo view of the $2mF_o - DF_c$ electron density map and fitted structure for the YL128H RC (yellow carbons), showing B_A and residue His L128. Orange dots indicate a putative hydrogen bond. (C) Stereo view of the $2mF_o - DF_c$ electron density map and fitted structure for the FL146A RC (yellow carbons), showing B_A and the Ala L146 residue. (D) Same view as in part C of the WT RC (cyan carbons).

electron density map and fitted structure for B_A (left, background) and an Ala residue at the L146 position (right, foreground); the space between the methyl group of Ala L146 and the acetyl C═O (distance 7.8 Å) would normally be occupied by the remainder of a Phe side chain in the structure of the WT RC, as shown in Figure 4D. This space was devoid of any density that could be modeled as a water molecule, so in the final structure of the FL146A RC, the cavity was empty. This left open the question of whether this mutation had achieved the introduction of a hydrogen bond to the acetyl carbonyl of B_A, as the cavity could well accommodate one or more disordered water molecules, but it was possible to conclude that the structural effects of the mutation were confined to the immediate vicinity of this carbonyl group, and therefore any change in the spectroscopic

properties of the FL146A RC are likely to stem from a change in the properties of B_A.

As an aside, both new X-ray crystal structures included electron density that supported modeling of the Q_B ubiquinone in the so-called proximal position (not shown), and large numbers of waters (341 for YL128H and 238 for FL146A). Neither density map included a feature that could be modeled as a lipid, but both contained surface electron density that could be modeled as LDAO (nine for YL128H and five for FL146A) or an alkane chain (two for FL146A).

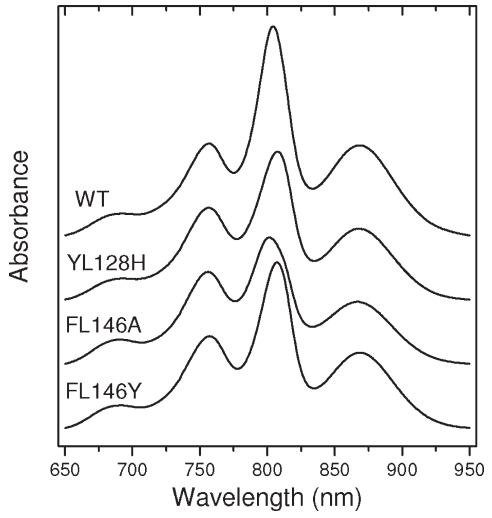

Figure 5. Room temperature absorbance spectra of membrane-bound RCs with mutations selectively affecting the acetyl carbonyl of B_A. Spectra were corrected for background scatter from the membrane between 650 and 950 nm and normalized to the same absorbance at 756 nm for comparison.

Further support for an impact of the YL128H and FL146A mutations on the properties of B_A was provided by their absorbance spectra (Figure 5, recorded for RCs in antenna-deficient membranes). In the YL128H and FL146Y RCs, the absorbance band of the accessory BChls, which had a maximum at 804 nm in the spectrum of the WT RC, was somewhat diminished in relative intensity and its maximum was red-shifted to 807 nm. In the spectrum of the FL146A RC, this band was further diminished and its maximum was blue-shifted to 802 nm, with some evidence of a shoulder at around 810 nm. In contrast, the maxima of the absorbance bands attributable to the RC BPhes at around 756 nm and the P BChls at 868 nm were not significantly affected by the mutations. Thus, the spectra supported a selective effect of the three mutations on the adjacent B_A BChl.

Charge Recombination Kinetics. Figure 6 shows the temporal evolution of absorption changes at 690 nm within a 20 ns window following excitation at 532 nm of antenna-deficient membranes containing WT or mutant *Rba. sphaeroides* RCs with blocked electron transfer to Q_A. A transient signal from the broad absorption band of H_A^- is expected at 690 nm, with possibly a small admixture of the signal from P^+.[16,54,55] The state $P^+H_A^-$ is formed on a time scale up to a few tens of picoseconds in the different types of RC,[34,39,41−44,52] which is much faster than the temporal resolution of the presented data. If the state $P^+H_A^-$ is in equilibrium with $P^+B_A^-$, as has often been proposed,[10,15,16,56−58] there should be an additional positive contribution of the transient signal from B_A^- at 690 nm.[59] Moreover, this contribution may be modulated by any mutation-related shift in the equilibrium between $P^+H_A^-$ and $P^+B_A^-$ and slight changes in the

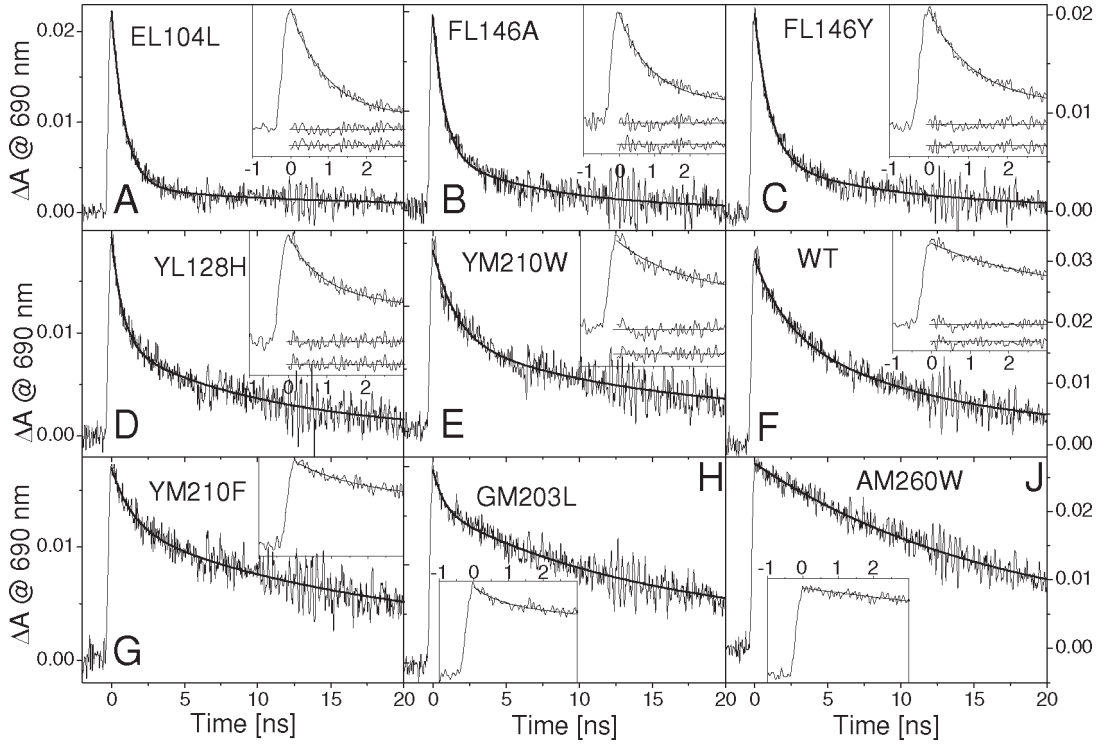

Figure 6. Absorption changes at 690 nm over a 20 ns temporal window induced by picosecond excitation at 532 nm. Absorption changes reflect the kinetics of formation and decay of the state $P^+H_A^-/P^+B_A^-$. Insets show the same absorption changes over the first 3 ns with, for panels A−F, the residuals for two-exponential fits (upper traces) and for three-exponential fits (lower traces). The fit parameters are given in Tables 2 and 3.

Table 2. Biexponential Fit Parameters Describing the Time Dependence of Absorbance Changes at 690 nm[a]

RC	τ_1 (ns) A_1	τ_2 (ns) A_2	τ_{av} (ns) $A_1 + A_2$	const
EL104L	**0.9**	**13**	**2.2**	
	0.87	0.1	0.97	0.03
FL146A	**0.8**	**7.4**	**2.7**	
	0.71	0.28	0.99	0.01
FL146Y	**1**	**9.3**	**3**	
	0.75	0.24	0.99	0.01
YL128H	**0.8**	**11**	**5.4**	
	0.54	0.45	0.99	0.01
YM210W	**1.5**	**14**	**7.5**	
	0.48	0.44	0.92	0.08
WT	**2.1**	**11**	**7.7**	
	0.35	0.59	0.94	0.06
YM210F	**1.4**	**17**	**11.6**	
	0.3	0.57	0.87	0.13
GM203L	**0.7**	**15**	**11.5**	
	0.2	0.62	0.82	0.18
AM260W		**17**	**17**	
		0.9	0.9	0.1

[a] The fitting function was $\Delta A = \Sigma A_i \exp(-t/\tau_i)$ + const, where ΣA_i + const = 1 (normalization). Fitting was performed in a 100 ns temporal window. For each sample, an average lifetime was calculated from the formula $\tau_{av} = \Sigma A_i \tau_i / \Sigma A_i$. Only a single exponential function was resolved for the AM260W RC.

Table 3. Three-Exponential Fit Parameters Describing the Time Dependence of Absorbance Changes at 690 nm[a]

RC	τ_1 (ns) A_1	τ_2 (ns) A_2	τ_3 (ns) A_3	const
EL104L	**0.5**	**1.2**	**15**	
	0.36	0.53	0.08	0.03
FL146A	**0.43**	**1.7**	**9.4**	
	0.43	0.37	0.19	0.01
FL146Y	**0.49**	**1.6**	**11**	
	0.31	0.48	0.2	0.01
YL128H	**0.41**	**1.4**	**11**	
	0.31	0.27	0.41	0.01
YM210W	**0.38**	**3.2**	**16**	
	0.26	0.35	0.32	0.07
WT	**0.37**	**3.3**	**12**	
	0.14	0.32	0.48	0.06

[a] The fitting function was $y = \Sigma A_i \exp(-t/\tau_i)$ + const, where ΣA_i + const = 1 (normalization). Fitting was performed in a 100 ns temporal window.

B_A/B_A^- spectrum. In line with these expectations, a positive signal appeared immediately after excitation due to formation of the radical pair $P^+H_A^-$ (and $P^+B_A^-$), followed by a slow decay attributable to $P^+H_A^-/P^+B_A^- \rightarrow PB_AH_A$ charge recombination. Charge recombination may also lead to formation of a triplet state ^3P of the primary electron donor in a minor fraction of RCs, and a small long-lived component attributable to this triplet state was observed at 690 nm in some of the samples (see below).

Interestingly, the kinetics of charge recombination were modulated differently by each of the mutations under study (Figure 6). In the EL104L, FL146A, FL146Y, YL128H, and YM210W mutants, the average lifetime, τ_{av}, of charge recombination was shorter than in the WT, whereas, in the YM210F, GM203L, and AM260W mutants, it was longer (Table 2, column 4). The slowest charge recombination was measured for AM260W, the only mutant constructed in order to remove quinone Q_A,[19,20] and not to specifically modulate the free energy gap between the states $P^+H_A^-$ and $P^+B_A^-$. The likely reason for this is explored below.

In all of the RCs tested, except for AM260W, transient absorption at 690 nm decayed in a clearly nonmonoexponential manner within the first 100 ns after excitation. Two-exponential fits approximated the experimental kinetics quite well (Figure 6A−H and Table 2, columns 2 and 3), but in the case of the YL128H, YM210W, and WT RCs, the quality of the two-exponential fits was insufficient as judged by the residuals (Figure 6D−F) and three-exponential fits (Table 3) were necessary in order to significantly decrease structure in the residuals within the first few nanoseconds after excitation (compare the residuals for two- and three-exponential fits in the insets to Figure 6D−F). In the three mutants characterized by the fastest overall charge recombination kinetics (EL104L, FL146A, and FL146Y), the improvement of the fit quality after addition of the third component was small (Figure 6A−C and Table 3), and so the necessity of this added complexity was uncertain. The fastest kinetic component in the three-exponential fits was of the order of 0.4−0.5 ns (Table 3), comparable with the width of the response function of the instrument used. Given this, and the fact that the fits were performed without deconvolution of the instrument response function, the exact values of this lifetime component and the associated amplitudes were somewhat uncertain. Three-exponential fits with similar lifetimes to those presented in Table 3 were reported previously for $P^+H_A^- \rightarrow PH_A$ charge recombination kinetics measured with picosecond resolution for isolated RCs from WT *Rba. sphaeroides*.[16]

Two-Exponential Fits. A comparison of the lifetimes and amplitudes obtained in the two-exponential fits of the experimental data is presented graphically in Figure 7A and B, respectively. The distribution of lifetimes for the different RC preparations on a logarithmic scale (Figure 7A) was similar for the fast and slow kinetic components: in both cases, the shortest lifetime was ∼2−3 times smaller than the respective longest lifetime (0.7−2.1 ps for τ_1 and 7.4−17 ns for τ_2; see Table 2 for exact values). Interestingly, the four "fastest" mutant RCs (EL104L, FL146A, FL146Y, and YL128H) were characterized by a similar τ_1 lifetime of 0.8−1.0 ns, whereas τ_1 increased to 1.4−2.1 ns in the case of three slower RCs (YM210W, WT, and YM210F) and, unexpectedly, decreased to 0.7 ns for the "slow" GM203L RC (Table 2). The three "slow" mutant RCs (YM210F, GM203L, and AM260W) were characterized by a τ_2 lifetime that was longer than the τ_2 lifetime for all the remaining RCs.

Although the effect of the different mutations on the τ_1 and τ_2 lifetimes was moderate, the relative amplitudes associated with the lifetimes were modulated very strongly (Figure 7B). The amplitude of the fast component (A_1) ranged from 0.87 for the fastest mutant (EL104L) to 0.00 for the slowest mutant (AM260W) and correlated well with the average lifetime τ_{av} for the recombination (Figure 8A, black squares). As expected, the amplitude of the slow component (A_2) behaved oppositely and increased from 0.10 for the fastest mutant to 0.90 for the slowest mutant. Thus, the marked differences in the charge recombination kinetics for the different RCs presented in Figure 6 were

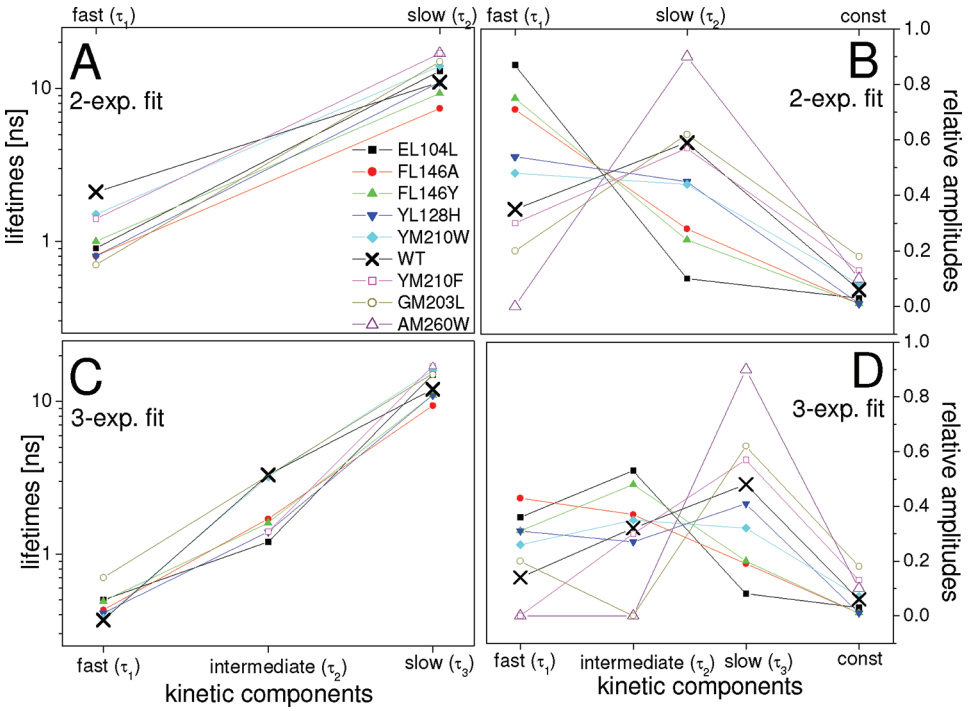

Figure 7. Graphical comparison of kinetic lifetime and amplitude components. Panels show lifetimes (A and C) and relative amplitudes (B and D) of the components obtained in two-exponential fits (A and B) and three-exponential fits (C and D) of absorption changes at 690 nm in the nine RCs. The kinetics are shown in Figure 6, and the lifetimes and relative amplitudes are listed in Tables 2 and 3.

caused mainly by modulation of the relative contributions of the fast and slow phases, and only to a minor extent by modulation of the actual values of the lifetimes.

The amplitude of the nondecaying component observed on a 100 ns time scale generally increased in parallel with the average lifetime (Figure 7B and Table 2, last column). In order to reveal the nature of this long-lived component, fits of all experimental traces were also performed over a 6 μs time scale (Table 4). This procedure allowed resolution of a slow component with a lifetime (τ_3) of 3.4−7.4 μs for the five slowest RCs (YM210W, WT, YM210F, GM203L, AM260W), and this is attributed to the decay of the triplet state, ^{3}P.[10,15,18] Moreover, a small contribution of an ∼300 ns component was found in the case of two slow mutants (YM210F, GM203L) and one fast mutant (EL104L). It was concluded that there was no substantial formation of the P^3 triplet state in those RCs that displayed relatively fast charge recombination.

Three-Exponential Fits. Figure 7C and D show a graphical comparison of lifetimes and amplitudes obtained from three-exponential fits of the experimental data over a 100 ns window. In addition to the data for the six "fastest" RCs detailed in Table 3 and described above, lifetimes and amplitudes of three "slowest" mutants fitted with only one (AM260W) or two exponential functions (YM210F and GM203L; Table 2) are shown for comparison. For these three slowest mutants, we could not resolve additional faster phases when trying fits with more exponential functions. In Figure 7C, for the biphasic GM203L RC, the shorter lifetime was plotted as τ_1 (sub-ns) and the longer lifetime as τ_3 (∼10−20 ns), while, for the biphasic YM210F RC, the shorter lifetime was plotted as τ_2 (few ns) and the longer lifetime as τ_3. The single lifetime for the AM260W RC was plotted as τ_3 (∼10−20 ns). In Figure 7D, the amplitudes of the one missing component for the YM210F and GM203L RCs and the two missing components for the AM260W RC were set to zero.

Scrutiny of the lifetime of the fastest phase (τ_1) showed that its distribution across the different RCs was very narrow (0.37−0.50 ns, with only the 0.7 ns lifetime taken from a two-exponential fit for GM203L RC being somewhat larger; Figure 7C, Tables 3 and 2). Also, the distribution of τ_3 was quite narrow (Figure 7C). On the other hand, τ_2 was grouped into two clusters, from 1.2 to 1.7 ns for most of the RCs and 3.2 to 3.3 ns for the YM210W and WT complexes. The amplitudes of the slowest component (Figure 7D) followed the pattern observed for the amplitudes of the slow phase in the two-exponential fits (Figure 7B), in that the slower the overall charge recombination, the bigger the amplitude of this component. On the other hand, amplitudes associated with the fast and intermediate phases generally decreased with increasing average lifetime of charge recombination, as was observed for the amplitude of the fast component in the two-exponential fits.

DISCUSSION

Multiexponential kinetics for decay of the primary radical pair, $P^+H_A^-$, have previously been rationalized through two competing, but not mutually exclusive, models. According to the relaxation model,[21,60] the free energy of the state $P^+H_A^-$ is proposed to decrease with time due to the reorganization of nuclei that slowly adapt to the dipolar electrostatic field caused by the appearance of $P^+H_A^-$. This relaxation occurs on a time scale that is shorter than the lifetime of $P^+H_A^-$ in closed RCs, leading to a distribution of lifetimes of $P^+H_A^-$ as the free energy gap between P* and $P^+H_A^-$ increases with time. According to the alternative model, the source of the different lifetimes for recombination is structural heterogeneity within the RC population.[15−17] In this model, transitions between coexisting conformers of the RC occur on a time scale that is longer than the

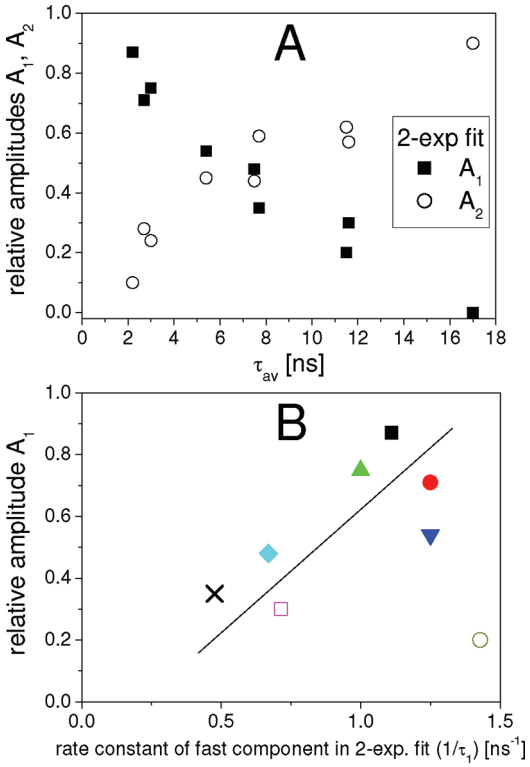

Figure 8. Correlations between fit parameters. (A) Relationship between the relative amplitudes of the fast (A_1) and slow (A_2) components in two-exponential fits and the average charge recombination lifetime (τ_{av}) for nine different RCs (values taken from Table 2). (B) Correlation between the relative amplitude (A_1) and rate constant ($1/\tau_1$) of the fast component in two-exponential fits for eight of the RCs studied (values taken from Table 2). Symbols for all samples are as for Figure 7.

lifetime of the state $P^+H_A^-$, and thus are not related to modulation of intraprotein electrostatic field by appearance and decay of $P^+H_A^-$.

The data presented in this paper favor the relaxation model, the main argument being that different mutations strongly affect the relative amplitudes of the different phases but have a much smaller effect on the lifetimes of the phases. In the framework of the heterogeneity model, one would expect that mutations designed to modulate the free energy gap between $P^+H_A^-$ and $P^+B_A^-$, but not to change the ratio between different RC conformers, would affect the lifetimes of decay (due to changes in free energy gaps) and not the amplitudes associated with these lifetimes (which are dictated by the relative concentrations of the different conformers). Of course, we cannot completely exclude the possibility that a side effect of the mutations employed in this study is a strong modulation of the concentrations of particular conformers. However, analysis of locations of the mutated amino acids, which are rather distant from Q_A (except for Glu L104; Figure 1A), leads to the conclusion that it is rather unlikely that these mutations cause significant changes in screening of the charge on Q_A, differences in this being one proposed source of structural heterogeneity.[15,16] Furthermore, the relaxation model, together with the idea that $P^+H_A^-$ decays via the state $P^+B_A^-$, provides a simple and elegant explanation of the observed modulation of the relative amplitudes of the different kinetic phases of the recombination, as discussed below.

The primary goal of the mutations chosen or constructed for this project was to modulate the free energy gap between $P^+H_A^-$ and $P^+B_A^-$. According to a picture where $P^+H_A^-$ recombines via a thermally activated $P^+B_A^-$ state, modulation of the free energy gap between these states should result also in modulation of the charge recombination kinetics. The results shown in Figure 6 were in full accord with the predictions of this model. All mutations predicted to decrease (EL104L, FL146A, FL146Y, and YL128H) or increase (GM203L) this free energy gap (Figure 3) indeed accelerated and decelerated, respectively, the overall kinetics (characterized by the average lifetime) (Table 2 and Figure 6). Somewhat unexpectedly, however, the lifetimes of particular phases in the multiexponential fits were influenced by the mutations only to a minor extent, and the marked changes in kinetics shown in Figure 6 were mostly due to modulation of the amplitudes, as depicted in Figure 7. This raises the question of how the small changes in lifetimes (and thus in the free energy gaps between $P^+H_A^-$ and $P^+B_A^-$ caused by the mutations) can be rationalized with large changes in the amplitudes of the components and in the overall kinetics. The answer to this question is offered by a model combining relaxation of the free energy of $P^+H_A^-$ relative to that of $P^+B_A^-$ with a thermally activated decay of $P^+H_A^-$ via $P^+B_A^-$.

The first indication that such a model may be appropriate comes from the observation of a correlation between the relative amplitudes (A_1) and rate constants ($1/\tau_1$) of the most rapid component in the two-exponential fits (Table 2). This correlation (Figure 8B) indicates that, with the exception of the GM203L mutant, the faster the rapid charge recombination phase, the bigger is its amplitude. A plausible explanation for this is that there is a competition between $P^+H_A^-$ charge recombination via $P^+B_A^-$ and relaxation of $P^+H_A^-$ to a more slowly decaying form, termed $(P^+H_A^-)_{rel}$.

Figure 9 shows a working model for the recombination of $P^+H_A^-$ by this mechanism, with either one or two relaxation steps included depending on whether two- or three-exponential fits are required to describe the data. For simplicity, possible direct transitions from all forms of the state $P^+H_A^-$ to the ground

Table 4. Results of the Fitting Procedure Performed over a 6 μs Time Scale with up to Three Exponential Functions

RC	τ_1 (ns) A_1	τ_2 (ns) A_2	τ_3 (ns) A_3	const
EL104L	**0.9**	**11**	**290**	
	0.87	0.1	0.02	0.01
FL146A	**0.43**	**1.7**	**9.4**	
	0.43	0.37	0.19	0.01
FL146Y	**0.49**	**1.6**	**11**	
	0.31	0.48	0.2	0.01
YL128H	**0.41**	**1.4**	**11**	
	0.31	0.27	0.41	0.01
YM210W	**2.5**	**16**	**3700**	
	0.56	0.38	0.06	0
WT	**2.6**	**13**	**7400**	
	0.4	0.55	0.03	0.02
YM210F	**13**	**300**	**6800**	
	0.82	0.07	0.11	0
GM203L	**13**	**360**	**4900**	
	0.77	0.07	0.16	0
AM260W		**19**	**3500**	
		0.89	0.09	0.02

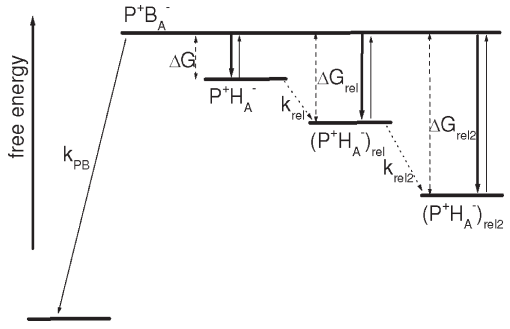

Figure 9. Free energy scheme of the relaxation model explaining the observed multiexponentiality of $P^+H_A^- \rightarrow PH_A$ charge recombination. See text for details. It should be emphasized that in the frame of the relaxation model the states $(P^+H_A^-)_{rel}$ and $(P^+H_A^-)_{rel2}$ are accessible from the state $P^+B_A^-$ only after the respective relaxation steps. For simplicity, the scheme does not show the variation of the free energy gaps between the different preparations studied, which explains the observed variation of the recombination kinetics.

(or triplet) state have been omitted, as these are assumed to be relatively slow. It was established that incorporation of these extra decay routes could be achieved without affecting the main conclusions (data not shown).

In the model presented in Figure 9, experimentally measured lifetimes (τ_1, τ_2, and τ_3; Tables 2 and 3) are assigned to different forms of the primary radical pair which are denoted $P^+H_A^-$ and $(P^+H_A^-)_{rel}$ (and $(P^+H_A^-)_{rel2}$ in the case of three-exponential fits). Thus, the rate constant of the fastest phase, k_1 (=$1/\tau_1$) is calculated as a sum of two decay rates, termed $k_{PH}(k_{PB}, \Delta G)$ and k_{rel}, that represent two competing pathways of decay of $P^+H_A^-$:

$$k_1 = k_{PH}(k_{PB}, \Delta G) + k_{rel}$$

For clarity, the rate $k_{PH}(k_{PB}, \Delta G)$ (see the Appendix for the formulas) is not explicitly shown in Figure 9. This rate represents decay of the state $P^+H_A^-$ via $P^+B_A^-$ and thus depends on the values of the decay rate k_{PB} and the free energy gap ΔG. On the basis of the experimentally measured lifetimes and amplitudes (Tables 2 and 3), it is possible to calculate the rate constant for relaxation k_{rel} (and k_{rel2} for three-exponential fits) and for charge recombination of both nonrelaxed and relaxed forms of $P^+H_A^-$ via $P^+B_A^-$, these being $k_{PH}(k_{PB}, \Delta G)$, $k_{PHrel}(k_{PB}, \Delta G_{rel})$, and $k_{PHrel2}(k_{PB}, \Delta G_{rel2})$ (see the Appendix). Assuming a value for k_{PB}, it is then possible to calculate the free energy gaps between $P^+H_A^-$ and $P^+B_A^-$ for all the RCs and all the states of relaxation. The results of all these calculations, assuming a value of k_{PB} = 5 ns^{-1},[16,61] are collected in Table 5, with rates represented as lifetimes. In principle, we cannot exclude the possibility that the rate k_{PB} is modulated to some extent by the mutations, especially those affecting BChl B_A. However, for the purposes of the model, it was assumed that this modulation is small and it was not included, except for the GM203L mutant (see below).

In modeling based on a two-exponential fit to the experimental data (Table 5), values of τ_{PH} increased gradually from 1.0 ns (EL104L) to 6.1 ns (WT) in parallel with gradual increase of τ_{av} (Table 2). This increase of τ_{PH} resulted directly from the gradual changes in ΔG from 35 to 85 meV (eqs A5 and A6 of the Appendix), in line with expectations of the effects of the mutations summarized in Figure 6. For the two "slow" mutants, YM210F and GM203L, τ_{PH} and thus ΔG (calculated for k_{PB} = 5 ns^{-1} [16,61]) are both smaller than those for the WT. These unexpectedly small values for ΔG, especially for the GM203L RC, can be easily increased to 86−96 meV if one assumes a higher value for k_{PB} (k_{PB} = 10−15 ns^{-1}). A value for ΔG for the GM203L RC that is higher than that for WT RC is expected due to the removal of a hydrogen bond from B_A (Figure 3). An additional effect of this mutation may well be an acceleration of k_{PB}, since the mutation affects B_A (via its keto carbonyl group). Although three other mutations also affect B_A (FL146A, FL146Y, YL128H), all of them are located near the acetyl carbonyl group of B_A, which may have no effect on k_{PB}.

Another important parameter of the model depicted in Figure 9 is the rate of $P^+H_A^-$ relaxation k_{rel}, represented in Table 5 as the relaxation time, τ_{rel}. This is the time needed to increase the free energy gap between $P^+H_A^-$ and $P^+B_A^-$ from ΔG to ΔG_{rel} in the absence of competing decay of $P^+H_A^-$ via $P^+B_A^-$. Except for extremely fast relaxation in the GM203L RC (τ_{rel} = 0.9 ns) and extremely slow relaxation for EL104L (τ_{rel} = 6.9 ns), values of τ_{rel} changed at most by a factor of ~2 (1.7−4 ns) in all the remaining RCs. This finding is interpreted as showing that most of the mutations do not affect the rate of relaxation significantly. However, the two extreme cases suggest that a significant modulation of τ_{rel} is possible in either direction. This is not surprising if one considers that the source of relaxation is likely to be nuclear reorganization of amino acids that neighbor the electron transfer cofactors, and that substitution of one of these amino acids may influence the rate of this reorganization. In previous work, it has been suggested that the rate of relaxation may be modulated by the electrostatic field originating from the charge on Q_A^- and possibly from additional charges associated with protonatable side chains of nearby amino acids.[16] In the light of the present findings, we propose that the nature of both the electrostatic environment and the amino acids in the vicinity of electron transfer cofactors influences the relaxation time τ_{rel}. In line with this, the lack of the fast phase in the mutant AM260W that lacks a Q_A quinone, and hence lacks the negative charge on Q_A (Table 2, Figure 6), may be interpreted as a manifestation of extremely fast relaxation ($\tau_{rel} \rightarrow 0$) in the absence of an electrostatic field from Q_A^-. Alternatively, there may be no temporal evolution of the size of the free energy gap between $P^+H_A^-$ and $P^+B_A^-$ (i.e., no relaxation) in Q_A-removed RCs. Finally, the situation for Q_A-removed RCs may not be comparable with that for Q_A-reduced RCs. The slow relaxation (high value of τ_{rel}) for the EL104L RC may be related to the fact that this is the only mutation in this study that (1) changes selectively the properties of H_A and (2) is located between H_A and Q_A. On the other hand, one may speculate that the extremely fast relaxation of $P^+H_A^-$ seen for the GM203L RC (τ_{rel} = 0.9 ns) is related to a unique characteristic of this mutation (see remarks above on a possible unique influence of this mutation on k_{PB}). Since this mutation affects selectively B_A, one needs to keep in mind that the microscopic phenomena underlying the process of relaxation (e.g., nuclear reorganization, influence of the electrostatic field) may affect both the states $P^+H_A^-$ and $P^+B_A^-$.

The fourth calculated parameter, ΔG_{rel} (Table 5), is directly related to the lifetime τ_2 (Table 2) and k_{PB} (eq A7 in the Appendix; $k_{PB} = 1/\tau_{PB}$). As with τ_2, the calculated relaxed free energy gap ΔG_{rel} was rather weakly dependent on the mutations, and significantly less so than the unrelaxed ΔG (Table 5). However, qualitatively, there was a similar correlation between both these gaps and τ_{av}, the average lifetime of $P^+H_A^-$, characterizing the overall effects of the mutations. Figure 10 shows that both ΔG and ΔG_{rel} generally decreased with decreasing τ_{av}.

Table 5. Parameters of the Model Presented in Figure 9[a]

	two-exponential fit				three-exponential fit						
strain	τ_{PH} (ns)	τ_{rel} (ns)	ΔG (meV)	ΔG_{rel} (meV)	τ_{PH} (ns)	τ_{rel} (ns)	τ_{PHrel} (ns)	τ_{rel2} (ns)	ΔG (meV)	ΔG_{rel} (meV)	ΔG_{rel2} (meV)
EL104L	1.0	6.9	35	104	1.4	0.78	1.5	7.0	45	47	108
FL146A	1.1	2.8	38	90	1.0	0.75	2.6	4.8	35	62	96
FL146Y	1.3	4.0	43	95	1.6	0.71	2.3	5.3	49	59	100
YL128H	1.5	1.7	47	100	1.3	0.59	3.6	2.3	43	71	100
YM210W	3.1	2.9	67	106	1.5	0.51	6.7	6.1	47	87	109
WT	6.1	3.2	85	100	2.7	0.43	8.7	5.3	63	94	102
YM210F	4.7	2.0	78	110							
GM203L	3.2	0.9	68	108							
AM260W				111							

[a] τ_{PB} was fixed at 200 ps. See the Appendix for the formulas.

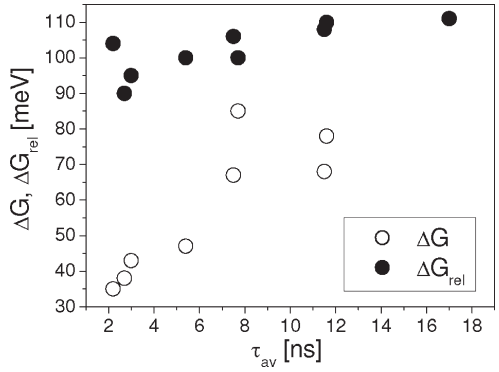

Figure 10. Correlation between the free energy gaps between $P^+B_A^-$ and $P^+H_A^-$ calculated on the basis of two-exponential fitting (ΔG and ΔG_{rel} - Figure 9, Table 5) and average $P^+H_A^-$ lifetime (τ_{av} - Table 2).

This observation further validates our "relaxation/thermally activated" model, showing that the theoretically predicted effects of the mutations on the free energy gaps between $P^+H_A^-$ and $P^+B_A^-$ are observed both in nonrelaxed and relaxed states of the RC, although the effect is small in the latter case (Figure 10, closed symbols). The relatively weak dependence of ΔG_{rel} on τ_{av} may be explained by a contribution of direct recombination of the relaxed radical pair $(P^+H_A^-)_{rel}$ (without intermediate formation of the state $P^+B_A^-$) seen on a longer time scale.

The model presented in Figure 9 assumes that the relaxation is an irreversible process. On the other hand, for some strains, the calculated free energy gap between the unrelaxed and relaxed form of $P^+H_A^-$ is small enough to consider a thermal equilibrium between these states. In such a case, the observed lifetime τ_2 (in the two-exponential modeling) is an average of lifetimes of the two $P^+H_A^-$ states weighted by their Boltzmann contributions. We estimated that, for WT RCs, characterized by the smallest free energy gap between $P^+H_A^-$ and $(P^+H_A^-)_{rel}$ (15 meV, Table 5), including a possibility of thermal equilibrium between these two states would yield the intrinsic lifetime of $(P^+H_A^-)_{rel}$ of up to 18 ns (compared to 11 ns in our irreversible model; Table 2) and ΔG_{rel} of up to 112 meV (compared to 100 meV in the irreversible model; Table 5). The corrections due to the reversibility of relaxation for the other RCs are significantly smaller.

Parameters of the model shown in Figure 9 were also calculated for the three-exponential fits of the charge recombination kinetics in the five "fastest" mutant RCs and the WT complex (Table 5). Due to the limited temporal resolution of the instrument, the fastest lifetime components and their amplitudes and, in consequence, the values of the model parameters were more uncertain than was the case for the two-exponential fits (see above). In this modeling, there were two relaxation phases, one of which occurred on the subnanosecond time scale (τ_{rel} = 0.43−0.78 ns) and the other on the nanosecond time scale (τ_{rel} = 2.3−7.0 ns). The consequence of these two relaxation steps was a gradual increase of the free energy gap from ΔG = 35−63 meV via ΔG_{rel} = 47−94 meV to ΔG_{rel2} = 96−109 meV.

It should be emphasized that the relaxation process and relaxation times τ_{rel} and τ_{rel2} discussed here are related to the evolution of the free energy gap between the states $P^+H_A^-$ and $P^+B_A^-$, and so they are not identical to their counterparts related to evolution of the free energy gap between the states $P^+H_A^-$ and P*, observed in fluorescence.[18,21,60] In order to fully describe the process of relaxation, it would be necessary to compare the data described in the present report with time-resolved fluorescence measurements on the same set of RC complexes, and such studies are planned.

Unlike the EL104L (and YM210W and YM210F) mutant, in which the free energy of $P^+H_A^-$ relative to the ground state was modified as a result of the mutation, in four other cases (FL146A, FL146Y, YL128H, GM203L), the energy of the state $P^+H_A^-$ should have been unaffected, since these mutations selectively affect interactions of the monomeric BChl B_A with the surrounding protein (Figure 3). If this is indeed the case, then we can conclude that it is not the free energy gap between $P^+H_A^-$ and the ground state which predominantly modulates the rate of $P^+H_A^- \rightarrow PH_A$ charge recombination. This supports our model in which the electron transfer pathway $P^+H_A^- \rightarrow P^+B_A^- \rightarrow PB_AH_A$ is the main route of radical pair recombination in RCs with blocked electron transfer to Q_A. In order to estimate a possible contribution from direct $P^+H_A^- \rightarrow PH_A$ recombination without transient formation of the state $P^+B_A^-$, studies of the temperature dependence of this reaction would be required.

The physiological significance of accelerated $P^+H_A^-$ charge recombination in Q_A-reduced RCs seems to be quite obvious, providing a safe energy dissipation process under stress conditions that lead to accumulation of the Q_A^- state. It is well-known that this pathway competes with the formation of the harmful triplet state of P that can produce singlet oxygen.

Finally, we would like to point out that our simple modeling is based on the assumption that modulation of the electron transfer

kinetics in the mutant RCs is related solely to mutation-induced modification of the free energy levels of the relevant states. Although this view is well supported for most of the mutants under this study (see above), local changes of the environment as well as the changes in the coupling between cofactors might also contribute to the observed kinetics.[65]

APPENDIX

According to the model presented in Figure 9, the rate constants $k_{PH}(k_{PB}, \Delta G)$ and k_{rel} depict two competing pathways of $P^+H_A^-$ decay. Therefore, these two parameters are related to the lifetime τ_1 of the fastest phase found in the fitting procedure (Tables 2 and 3) by the formula

$$1/\tau_1 \equiv k_1 = k_{PH}(k_{PB}, \Delta G) + k_{rel} \quad (A1)$$

The ratio between the rate constants of the two competing pathways equals the ratio of the amplitudes of the fast phase (A_1) and a sum of the remaining amplitudes (A_2 + const for two-exponential fits and $A_2 + A_3$ + const for three-exponential fits). Therefore, for two-exponential fits, in simplified notation of $k_{PH} = k_{PH}(k_{PB}, \Delta G)$, one may write

$$k_{PH}/k_{rel} = A_1/(A_2 + \text{const}) \quad (A2)$$

Substituting in eq A1 k_{rel} with $1/\tau_{rel}$ and k_{PH} with the expression derived from eq A2, one obtains a formula for τ_{rel}:

$$\tau_{rel} = \tau_1/(A_2 + \text{const}) \quad (A3)$$

From eq A1, a formula for $\tau_{PH} \equiv 1/k_{PH}$ can be written:

$$\tau_{PH} = \tau_1\tau_{rel}/(\tau_{rel} - \tau_1) \quad (A4)$$

The rate k_{PH} (and thus the lifetime τ_{PH}) depends on the Boltzmann distribution between the states $P^+H_A^-$ and $P^+B_A^-$ and on the rate k_{PB} (Figure 9). It can be easily shown that

$$\tau_{PH}/\tau_{PB} = \exp(\Delta G/k_bT) + 1 \quad (A5)$$

where k_b is the Boltzmann constant and T is the absolute temperature. Derivation of the formula for ΔG from eq A5 is then

$$\Delta G = k_bT \ln[(\tau_{PH}/\tau_{PB}) - 1] \quad (A6)$$

The formula for ΔG_{rel} for two-exponential fits is similar to eq A6:

$$\Delta G_{rel} = k_bT \ln[(\tau_2/\tau_{PB}) - 1] \quad (A7)$$

For three-exponential fits, the formulas for τ_{PH} and ΔG are the same as for two-exponential fits (eqs A4 and A6, respectively) and the remaining parameters may be calculated from the formulas below:

$$\tau_{rel} = \tau_1/(A_2 + A_3 + \text{const}) \quad (A8)$$

$$\tau_{PHrel} = \tau_2\tau_{rel2}/(\tau_{rel2} - \tau_2) \quad (A9)$$

$$\tau_{rel2} = \tau_2(A_2 + A_3 + \text{const})/(A_3 + \text{const}) \quad (A8)$$

$$\Delta G_{rel} = k_bT \ln[(\tau_{PHrel}/\tau_{PB}) - 1] \quad (A10)$$

$$\Delta G_{rel2} = k_bT \ln[(\tau_3/\tau_{PB}) - 1] \quad (A11)$$

Accession Codes

Structures have been deposited in the Protein Data Bank under accession codes 3ZUW for the YL128H RC and 3ZUM for the FL146A RC.

AUTHOR INFORMATION

Corresponding Author

*Phone: +48 61 8296370. E-mail: krzyszgi@amu.edu.pl.

Present Addresses

[⊥]Current address: Centre for Biomolecular Sciences, University of St Andrews, North Haugh, St Andrews, Fife, KY16 9ST, United Kingdom.

[#]Current address: Division of Biological Chemistry and Molecular Microbiology, Faculty of Life Sciences, University of Dundee, Nethergate, Dundee, DD1 4HN, United Kingdom.

ACKNOWLEDGMENT

K.G. acknowledges financial support from the Polish government (project entitled "Electrostatic control of electron transfer in purple bacteria reaction center" no N N202 127 437). M.R.J., J. A.P., and P.K.F. acknowledge funding from the Biotechnology and Biological Sciences Research Council of the United Kingdom.

ABBREVIATIONS

B_A - accessory monomeric bacteriochlorophyll; BChl - bacteriochlorophyll; BPhe - bacteriopheophytin; H_A - acceptor BPhe; P - BChl dimer, primary electron donor; Q_A, Q_B - quinones; RC - reaction center; WT - wild-type

REFERENCES

(1) Woodbury, N. W. T.; Allen, J. P. Electron transfer in purple nonsulfur bacteria. In *Anoxygenic Photosynthetic Bacteria*; Blankenship, R. E., Madigan, M. T., Bauer, C. E., Eds.; Kluwer Academic Publishers: Dordrecht/Boston/London, 1995; p 527.

(2) Zinth, W.; Wachtveitl, J. *ChemPhysChem* **2005**, *6*, 871–880.

(3) Holzapfel, W.; Finkele, U.; Kaiser, W.; Oesterhelt, D.; Scheer, H.; Stilz, H. U.; Zinth, W. *Chem. Phys. Lett.* **1989**, *160*, 1–7.

(4) Holzapfel, W.; Finkele, U.; Kaiser, W.; Oesterhelt, D.; Scheer, H.; Stilz, H. U.; Zinth, W. *Proc. Natl. Acad. Sci. U.S.A.* **1990**, *87*, 5168–5172.

(5) Kirmaier, C.; Holten, D. *FEBS Lett.* **1988**, *239*, 211–218.

(6) Kirmaier, C.; Holten, D. *Biochemistry* **1991**, *30*, 609–613.

(7) Lockhart, D. J.; Kirmaier, C.; Holten, D.; Boxer, S. G. *J. Phys. Chem.* **1990**, *94*, 6987–6995.

(8) Rodriguez, J.; Kirmaier, C.; Johnson, M. R.; Friesner, R. A.; Holten, D.; Sessler, J. L. *J. Am. Chem. Soc.* **1991**, *113*, 1652–1659.

(9) Chan, C. K.; DiMagno, T. J.; Chen, L. X.; Norris, J. R.; Fleming, G. R. *Proc. Natl. Acad. Sci. U.S.A.* **1991**, *88*, 11202–11206.

(10) Shuvalov, V. A.; Parson, W. W. *Proc. Natl. Acad. Sci. U.S.A.* **1981**, *78*, 957–961.

(11) Schenck, C. C.; Blankenship, R. E.; Parson, W. W. *Biochim. Biophys. Acta* **1982**, *680*, 44–59.

(12) Chidsey, C. E. D.; Kirmaier, C.; Holten, D.; Boxer, S. G. *Biochim. Biophys. Acta* **1984**, *766*, 424–437.

(13) Ogrodnik, A.; Volk, M.; Letterer, R.; Feick, R.; Michel-Beyerle, M. E. *Biochim. Biophys. Acta* **1988**, *936*, 361–371.

(14) Tang, C. K.; Williams, J. C.; Taguchi, A. K. W.; Allen, J. P.; Woodbury, N. W. *Biochemistry* **1999**, *38*, 8794–8799.

(15) Gibasiewicz, K.; Pajzderska, M. *J. Phys. Chem. B* **2008**, *112* (6), 1858–1865.

(16) Gibasiewicz, K.; Pajzderska, M.; Ziółek, M.; Karolczak, J.; Dobek, A. *J. Phys. Chem. B* **2009**, *113* (31), 11023–11031.

(17) Volk, M.; Ogrodnik, A.; Michel-Beyerle, M. E. The recombination dynamics of the radical pair P^+H^- in external magnetic and electric fields. In *Anoxygenic Photosynthetic Bacteria*; Blankenship, R. E., Madigan, M. T., Bauer, C. E., Eds.; Kluwer Academic Publishers: Dordrecht/Boston/London, 1995; p 595.

(18) Woodbury, N. W. T.; Parson, W. W.; Gunner, M. R; Prince, R. C.; Dutton, P. L. *Biochim. Biophys. Acta* **1986**, *851*, 6–22.
(19) Ridge, J. P.; van Brederode, M. E.; Goodwin, M. G.; van Grondelle, R.; Jones, M. R. *Photosynth. Res.* **1999**, *59*, 9–26.
(20) McAuley, K. E.; Fyfe, P. K.; Ridge, J. P.; Cogdell, R. J.; Isaacs, N. W.; Jones, M. R. *Biochemistry* **2000**, *39*, 15032–15043.
(21) Woodbury, N. W. T.; Parson, W. W. *Biochim. Biophys. Acta* **1984**, *767*, 345–361.
(22) McPherson, P. H.; Okamura, M. Y.; Feher, G. *Biochim. Biophys. Acta* **1988**, *934*, 348–368.
(23) Marcus, R. A.; Sutin N. *Biochim. Biophys. Acta* **1985**, *811*, 265−322.
(24) McAuley-Hecht, K. E.; Fyfe, P. K.; Ridge, J. P.; Prince, S. M.; Hunter, C. N.; Isaacs, N. W.; Cogdell, R. J.; Jones, M. R. *Biochemistry* **1998**, *37*, 4740–4750.
(25) Jones, M. R.; Visschers, R. W.; van Grondelle, R.; Hunter, C. N. *Biochemistry* **1992**, *31*, 4458–4465.
(26) Jones, M. R.; Fowler, G. J. S.; Gibson, L. C. D.; Grief, G. G.; Olsen, J. D.; Crielaard, W.; Hunter, C. N. *Mol. Microbiol.* **1992**, *6*, 1173–1184.
(27) Jones, M. R.; Heer-Dawson, M.; Mattioli, T. A.; Hunter, C. N.; Robert, B. *FEBS Lett.* **1994**, *339*, 18–24.
(28) Otwinowski, Z.; Minor, W. *Methods Enzymol.* **1997**, *276*, 307–326.
(29) Navaza, J. *Acta Crystallogr., Sect. A* **1995**, *50*, 157–163.
(30) Collaborative Computational Project, Number 4. The CCP4 Suite: Programs for protein crystallography. *Acta Crystallogr., Sect. D* **1994**, *50*, 760−763.
(31) DeLano, W. L. *The PyMOL Molecular Graphics System*; DeLano Scientific: San Carlos, CA, 2002.
(32) Byrdin, M.; Thiagarajan, V.; Villette, S.; Espagne, A.; Brettel, K. *Rev. Sci. Instrum.* **2009**, *80*, 043102.
(33) Pawlowicz, N. P.; van Grondelle, R.; van Stokkum, I. H. M.; Jones, M. R.; Breton, J.; Groot, M. L. *Biophys. J.* **2008**, *95*, 1268–1284.
(34) Bylina, E. J.; Kirmaier, C.; McDowell, L.; Holten, D.; Youvan, D. C. *Nature* **1988**, *336*, 182–184.
(35) Lin, X.; Murchison, H. A.; Nagarajan, V.; Parson, W. W.; Allen, J. P.; Williams, J. C. *Proc. Natl. Acad. Sci. U.S.A.* **1994**, *91*, 10265–10269.
(36) Breton, J.; Nabedryk, E.; Allen, J. P.; Williams, J. C. *Biochemistry* **1997**, *36*, 4515–4525.
(37) Breton, J.; Bibikova, M.; Oesterhelt, D.; Nabedryk, E. *Biochemistry* **1999**, *38*, 11541–11552.
(38) Müh, F.; Williams, J. C.; Allen, J. P.; Lubitz, W. *Biochemistry* **1998**, *37*, 13066–13074.
(39) Schenkl, S.; Spörlein, S.; Müh, F.; Witt, H.; Lubitz, W.; Zinth, W.; Wachtveitl, J. *Biochim. Biophys. Acta* **2002**, *1554*, 36–47.
(40) Alden, R. G.; Parson, W. W.; Chu, Z. T.; Warshel, A. *J. Phys. Chem.* **1996**, *100*, 16761–16770.
(41) Potter, J. A.; Fyfe, P. K.; Frolov, D.; Wakeham, M. C.; van Grondelle, R.; Robert, B.; Jones, M. R. *J. Biol. Chem.* **2005**, *280*, 27155–27164.
(42) Jia, Y. W.; DiMagno, T. J.; Chan, C. K.; Wang, Z. Y.; Du, M.; Hanson, D. K.; Schiffer, M.; Norris, J. R.; Fleming, G. R.; Popov, M. S. *J. Phys. Chem.* **1993**, *97*, 13180–13191.
(43) Nagarajan, V.; Parson, W. W.; Davis, D.; Schenck, C. C. *Biochemistry* **1993**, *32*, 12324–12336.
(44) Beekman, L. M. P.; van Stokkum, I. H. M.; Monshouwer, R.; Rijnders, A. J.; McGlynn, P.; Visschers, R. W.; Jones, M. R.; van Grondelle, R. *J. Phys. Chem.* **1996**, *100*, 7256–7268.
(45) Visschers, R. W.; Vulto, S. I. E.; Beekman, L. M. P.; Jones, M. R.; van Grondelle, R.; Kraayenhof, R. *Photosynth. Res.* **1999**, *59*, 95–104.
(46) Parson, W. W.; Chu, Z. T.; Warshel, A. *Biochim. Biophys. Acta* **1990**, *1017*, 251–272.
(47) Gunner, M. R.; Nicholls, A.; Honig, B. *J. Phys. Chem.* **1996**, *100*, 4277–4291.
(48) Hamm, P.; Gray, K. A.; Oesterhelt, D.; Feick, R.; Scheer, H.; Zinth, W. *Biochim. Biophys. Acta* **1993**, *1142*, 99–105.
(49) Chan, C. K.; Chen, L. X. Q.; Di Magno, T. J.; Hanson, D. K.; Nance, S. L.; Schiffer, M.; Norris, J. R.; Fleming, G. R. *Chem. Phys. Lett.* **1991**, *176*, 366–372.
(50) Finkele, U.; Lauterwasser, C.; Zinth, W.; Gray, K. A.; Oesterhelt, D. *Biochemistry* **1990**, *29*, 8517–8521.
(51) Paddock, M. L.; Chang, C.; Xu, Q.; Abresch, E. C.; Axelrod, H. L.; Feher, G.; Okamura, M. Y. *Biochemistry* **2005**, *44*, 6920–6928.
(52) Shochat, S.; Arlt, T.; Francke, C.; Gast, P.; van Noort, P. I.; Otte, S. C. M.; Schelvis, H. P. M.; Schmidt, S.; Vijgenboom, E.; Vrieze, J.; Zinth, W.; Hoff, A. J. *Photosynth. Res.* **1994**, *40*, 55–66.
(53) McAuley, K. E.; Fyfe, P. K.; Cogdell, R. J.; Isaacs, N. W.; Jones, M. *FEBS Lett.* **2000**, *467*, 285–290.
(54) Parson, W. W.; Cogdell, R. J. *Biochim. Biophys. Acta* **1975**, *416*, 105–149.
(55) Gibasiewicz, K.; Pajzderska, M.; Karolczak, J.; Dobek, A. *Phys. Chem. Chem. Phys.* **2009**, *11*, 10484–10493.
(56) Kirmaier, C.; Gaul, D.; DeBey, R.; Holten, D.; Schenck, C. C. *Science* **1991**, *251*, 922–927.
(57) Heller, B. A. *Biochemistry* **1995**, *34*, 5294–5302.
(58) Heller, B. A.; Holten, D.; Kirmaier, C. *Biochemistry* **1996**, *35*, 15418–15427.
(59) Fajer, J.; Brune, D. C.; Davis, M. S.; Forman, M.; Spaulding, L. D. *Proc. Natl. Acad. Sci. U.S.A.* **1975**, *72*, 4956–4960.
(60) Hartwich, G.; Lossau, H.; Michel-Beyerle, M. E.; Ogrodnik, A. *J. Phys. Chem. B* **1998**, *102*, 3815–3820.
(61) Katilius, E.; Turanchik, T.; Lin, S.; Taguchi, A. K. W.; Woodbury, N. W. *J. Phys. Chem. B* **1999**, *103*, 7386–7389.
(62) Brűnger, A. T. *Nature* **1992**, *335*, 472–475.
(63) Cruickshank, D. W. J. *Acta Crystallogr., Sect. D* **1999**, *55*, 583–601.
(64) Laskowski, R. A.; MacArthur, W. W.; Moss, D. S.; Thornton, J. M. *J. Appl. Crystallogr.* **1993**, *26*, 283–291.
(65) Huppmann, P.; Arlt, T.; Penzkofer, H.; Schmidt, S.; Bibikova., M.; Dohse, B.; Oesterhelt, D.; Wachtveitl, J.; Zinth, W. *Biophys. J.* **2002**, *82*, 3186–3197.